Magnetically Tunable One-Dimensional Plasmonic

Photonic Crystals

Chaolumen Wu,[†] Qingsong Fan, [†] Wanling Wu,[‡] Tian Liang,[†] Yun Liu,[†] Huakang Yu, [‡] Yadong Yin*[†]

[†]Department of Chemistry, University of California, Riverside, CA 92521, USA

[‡]School of Physics and Optoelectronics, South China University of Technology, Guangzhou 510641, China

¹Hubei Key Laboratory of Radiation Chemistry and Functional Materials, School of Nuclear Technology and Chemistry & Biology, Hubei University of Science and Technology, Xianning 437100, China

KEYWORDS. Surface plasmon resonance, scattering, optical diffraction, magnetic assembly, one-dimensional, photonic crystals

ABSTRACT. Integrating plasmonic resonance into photonic bandgap nanostructures promises additional control over their optical properties. Here, one-dimensional (1D) plasmonic photonic crystals with angular-dependent structural colors are fabricated by assembling magneto-plasmonic colloidal nanoparticles under an external magnetic field. Unlike conventional 1D photonic crystals, the assembled 1D periodic structures show angular-dependent colors based on the selective activation of optical diffraction and plasmonic scattering. They can be further fixed in an elastic

polymer matrix to produce a photonic film with angular-dependent and mechanically tunable optical properties. The magnetic assembly enables precise control over the orientation of the 1D assemblies within the polymer matrix, producing photonic films with designed patterns displaying versatile colors from the dominant backward optical diffraction and forward plasmonic scattering. The combination of optical diffraction and plasmonic properties within a single system holds the potential for developing programmable optical functionalities for applications in various optical devices, color displays, and information encryption systems.

Many natural creatures can exploit the interaction of their micro- or nanostructures with light to produce vivid structural colors, which has inspired the development of a large number of functional photonic materials. 1-6 Such structurally colored materials are attractive due to their long-term stability, color tunability, and sustainable production, and are expected to have broad applications in colorimetric sensors, full-color display, information encryption, photonic pigment, and energy harvesting.⁷⁻¹² Diverse metallic and dielectric nanostructures have been developed to generate structural colors based on various physical phenomena, such as thin-film interference, light scattering, diffraction, and plasmonic resonance. 13-16 In particular, photonic crystals, periodically arranged nanoscale materials, can selectively reflect narrowband light with a strong dependence on the incident and observation angles.¹⁷ Plasmonic nanostructures, on the other hand, generate angular independent, low vibrancy colors due to the resonant interaction between light and metallic nanostructures, ¹⁸ allowing remarkable spectral tuning achievable by plasmonic coupling to display colors across the entire visible region.¹⁹ Featuring convenient control over the spatial configuration of the nanostructured building blocks, colloidal assembly strategies have been successfully used to modulate both types of structural colors. 19-21

Combining plasmonic resonance and photonic bandgap within a single system produces an intriguing optical active material: plasmonic photonic crystal, possessing unique and controllable optical properties from their synergetic effect. ²²⁻²³ Typically, photonic crystals have been used as structural motifs for metal deposition to produce plasmonic photonic crystals. ²²⁻²³ Kim et al. reported directional deposition of gold or aluminum on the photonic microspheres to generate Janus structures, showing plasmonic color from the top hemisphere while diffractive color from the bottom hemisphere. The two-color modes can be switched by the orientational control of the Janus microspheres using an external electric field. ²⁴ Omenetto et al. also reported plasmonic-photonic crystal hybrid nanostructures by depositing gold on a silk inverse opal, producing versatile optical properties by manipulating the interplay between photonic bandgap and surface plasmonic resonance. ²⁵ It is believed that incorporating active structural manipulation into such plasmonic photonic crystals will further enable the convenient and dynamic tuning of the two structural coloring mechanisms, resulting in novel optical materials with more exciting applications.

Magnetic actuation is appealing in fabricating responsive optical materials due to its fast response, reversibility, and remote control.²⁶⁻²⁸ Self-assembly of magnetic nanoparticles under an external magnetic field produces 1D periodic structures by balancing the electrostatic repulsion and magnetic attraction, creating a dynamically tunable photonic bandgap.²⁹⁻³⁰ In addition, magnetically tunable plasmon resonance has been demonstrated by assembling magnetoplasmonic hybrid nanostructures.³¹⁻³³ We previously reported magneto-plasmonic hybrid nanorods that could selectively excite the longitudinal and transverse plasmonic modes by dynamically controlling their orientation using external magnetic fields, thereby displaying different colors.³²

Developing magnetically responsive plasmonic photonic crystals is desirable as the dynamic manipulation of the interplay between photonic bandgap and plasmonic resonance promises the creation of programmable optical properties, which is a valuable feature for practical applications. In this work, we show that magneto-plasmonic nanoparticles can be assembled into 1D photonic crystals under an external magnetic field to display angular-dependent and dynamically tunable optical properties that take advantage of the different field-responsive behaviors of plasmonic scattering and optical diffraction. The convenient and robust magnetic assembly process further enables the fixation of the 1D plasmonic photonic crystals in an elastic polymer matrix to produce photonic films with angular-dependent, mechanically tunable, and multiple color patterns, which are promising for potential applications in color display, optical devices, and information encryption.

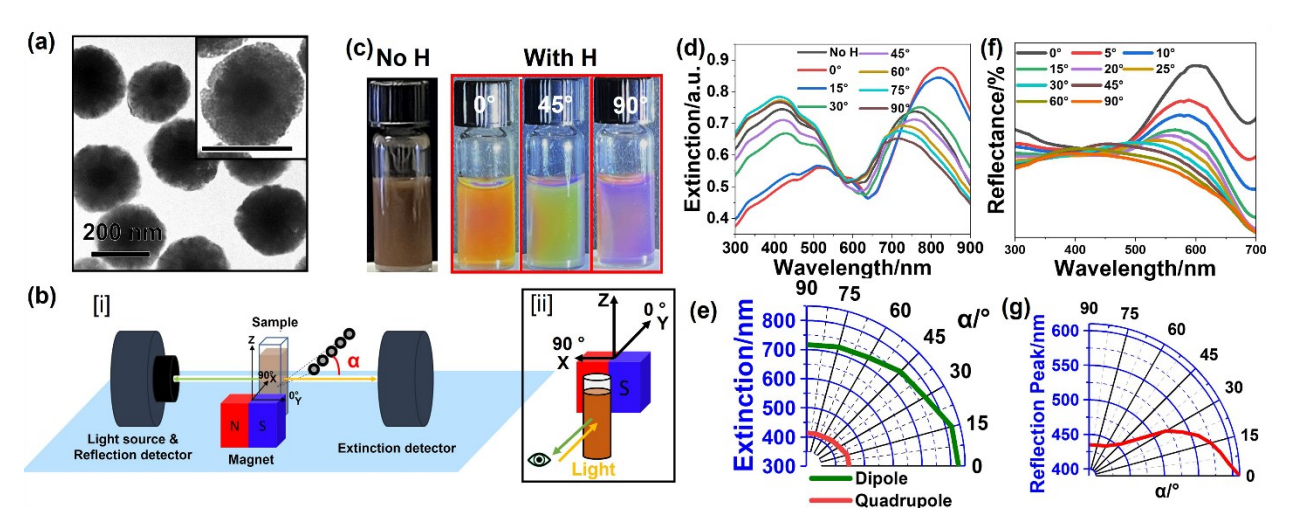


Figure 1. (a) TEM image of Ag@Fe₃O₄ nanoparticles. (b) Experimental setup for measuring extinction and reflection spectra [i] and observing the color of the nanoparticle solution [ii] under an external magnetic field from a cubic permanent magnet. (c) Photos of an aqueous solution of Ag@Fe₃O₄ nanoparticles before and after exposure to a magnetic field of varying directions (0, 45, 90°). (d) Extinction spectra of the nanoparticle solution under a magnetic field with varying α

from 0 to 90°. (e) Polar curve of the extinction peak shifts corresponding to the spectra in (d). (f) Reflectance spectra of the nanoparticle solution under a magnetic field with varying α from 0 to 90°. (g) Polar curve of the reflection peak shifts corresponding to the spectra in (f).

Magneto-plasmonic Ag@Fe₃O₄ core-shell nanoparticles with 80-nm Ag core and 75-nm thick Fe₃O₄ shell, as shown in the transmission electron microscopy (TEM) image in Figure 1a, were used as building blocks (Figure S1).³⁴ After surface modification with polyacrylic acid, they had high surface charges and good dispersibility in water so that they could be assembled into 1D nanochains with controllable orientation under external magnetic fields (Figure S3). Thanks to their strong magnetic property, the Ag@Fe₃O₄ nanoparticles can assemble into 1D chains within one second under an external magnetic field with a strength of 11 mT. As schematically illustrated in Figure 1b[i], the angle (α) between unpolarized incident light and the nanochains could be tuned from 0 to 90° by rotating the cubic magnet along the Z-axis in the XY plane (Video 1). When the nanoparticle solution was illuminated and observed along the Y-axis, as illustrated in Figure 1b[ii], it showed yellow, green, and light brown colors as α changed from 0 to 45 to 90° (Video 2). In contrast, it appeared dark brown without a magnetic field (Figure 1c), showing two extinction peaks, namely, a dipole and a quadrupole peak at 763 and 420 nm, respectively (black curve in Figure 1d and simulation in Figure S2). The extinction spectra in Figure 1d and the corresponding polar curve in Figure 1e shows that the quadrupole and dipole plasmonic peaks gradually blueshifted from 446 to 413 nm and from 827 to 717 nm, respectively, under an external magnetic field with a varying α from 0 to 90°. The reflection spectra in Figure 1f also showed a gradual blueshift of the diffraction peak from 610 to 455 nm as α increased from 0 to 45°. As α varied from 45 to 90°, a broader peak around 440 nm appeared, showing little dependence on α.

Finite-difference time-domain (FDTD) calculation was conducted to understand the angulardependent optical properties of the Ag@Fe₃O₄ nanochains. Figures 2a and b reveal a very good match between the experimental and the simulated results, including extinction spectra and the corresponding plasmonic peak shifts of the nanochains as α varied from 0 to 90°. We further performed detailed simulations on the two cases when $\alpha=90$ and 0°. When $\alpha=90$ °, as shown in Figures 2c and S4, the quadrupole plasmonic mode dominated the extinction spectra, with scattering mainly contributing to the extinction. The right panel maps the electric field distribution of a nanochain, indicating strong coupling between neighboring nanoparticles under 413 nm incident light, which greatly contributed to the strong plasmonic scattering. However, under this condition, the dipole plasmonic mode was greatly suppressed, and the dipole peak blueshifted due to the far-field plasmonic coupling between neighboring nanoparticles (Figure S5).³⁵ In contrast, when $\alpha=0^{\circ}$, the dipole plasmonic mode dominated, redshifting with greatly enhanced peak intensity (Figure 2d), while the quadrupole peak was significantly suppressed and redshifted. The electric field distribution of the nanochain in Figure 2d indicates that the Fe₃O₄ shells are also polarized, showing the electric dipole mode when incident light propagates along the nanochain. The interaction between the dipole modes of the Ag core and Fe₃O₄ shell and that of the neighboring nanoparticles may induce complex plasmonic coupling, producing the redshifted dipole and quadrupole peaks at $\alpha=0^{\circ}$. In short, the dipole plasmonic resonance dominated the extinction spectrum at $\alpha=0^{\circ}$, and quadrupole plasmonic resonance dominated at $\alpha=90^{\circ}$, attributed to different coupling modes, enabling angular-dependent optical properties. Furthermore, scattering always appeared stronger than absorption, which, when combined with optical diffraction, might contribute to interesting angle-dependent colors of the nanochain solutions.

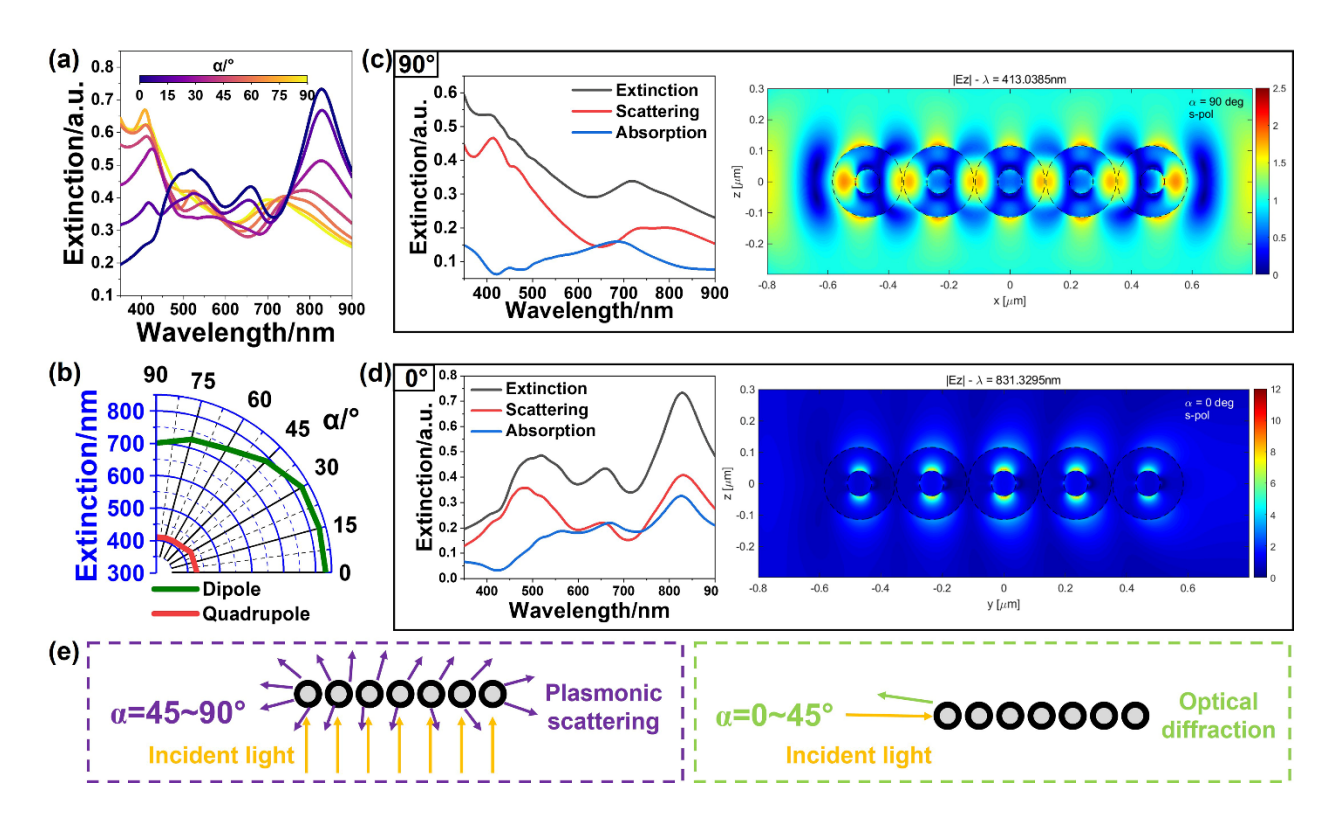


Figure 2. (a) Simulated extinction spectra and (b) the corresponding polar curve of the peak shifts of the Ag@Fe₃O₄ nanoparticle chains when α changes from 0 to 90°. (c, d) Simulated extinction spectra and electric field distributions of the Ag@Fe₃O₄ nanoparticle chains for $\alpha = 90^{\circ}$ (c) and $\alpha = 0^{\circ}$ (d). (e) Schematic illustration of the angular-dependent colors from the selective activation of plasmonic scattering and optical diffraction as α varies from 0 to 90°.

Control experiments were conducted to study the contribution of plasmonic scattering and optical diffraction. First, Fe₃O₄ shells were completely etched with oxalic acid, producing a pink dispersion of Ag nanoparticles with both extinction and reflection peaks at around 430 nm (Figure S6). Second, the Ag cores were removed by H₂O₂ etching to obtain a dispersion of Fe₃O₄ hollow nanospheres, which showed yellow, green, and reddish colors under external magnetic fields with varying directions from 0, 45, to 90° (Figure S7). The extinction peak shifted from 735 to 482 nm as α increased from 0 to 45° and remained constant at 482 nm for α above 45°. In contrast, the

reflection peak blueshifted from 567 to 444 nm as α increased from 0 to 45°, with no detection of any pronounced peaks when α was beyond 45°. Furthermore, simulations show that scattering dominates the extinction spectra of the Fe₃O₄ hollow nanosphere chains at both α =0 and 90°. These results suggest that the color of Fe₃O₄ hollow nanospheres was generated mainly from the optical diffraction as α varied from 0 to 45°. In contrast, scattering was the source of the color when α was larger than 45° (Figure S7e, f). Based on these control experiments and the above analysis, we conclude that optical diffraction dominates when α =0~45° and plasmonic scattering dominates when α =45~90° (Figure 2e), although the latter always contributes to the color of the Ag@Fe₃O₄ nanoparticle solution.

The angular-dependent diffraction of the 1D Ag@Fe₃O₄ nanoparticle assemblies was further confirmed by the photonic bandgap calculation. By inputting the experimental parameters into Bragg's Law ($m\lambda$ =2ndsin θ , with m being the order of diffraction, λ the diffraction wavelength, n the effective refractive index, d the lattice plane spacing, and θ the Bragg angle), we found that the colors were from the second-order diffraction (m=2) (see Supporting Information for detailed calculations). For confirming the applicability of the second-order diffraction at varying α , the d value was calculated by inputting the λ value from the reflection spectra into Bragg's Law (Figure S8), which was in a reasonable range when α varied from 0 to 45° but too large when α was over 45°, indicating the diffraction in the visible region was achievable only when $\alpha = 0$ ~45°. FDTD simulation of reflection spectra in Figure S9 also confirmed that reflection peaks in the visible region were observable only when $\alpha = 0$ ~45°.

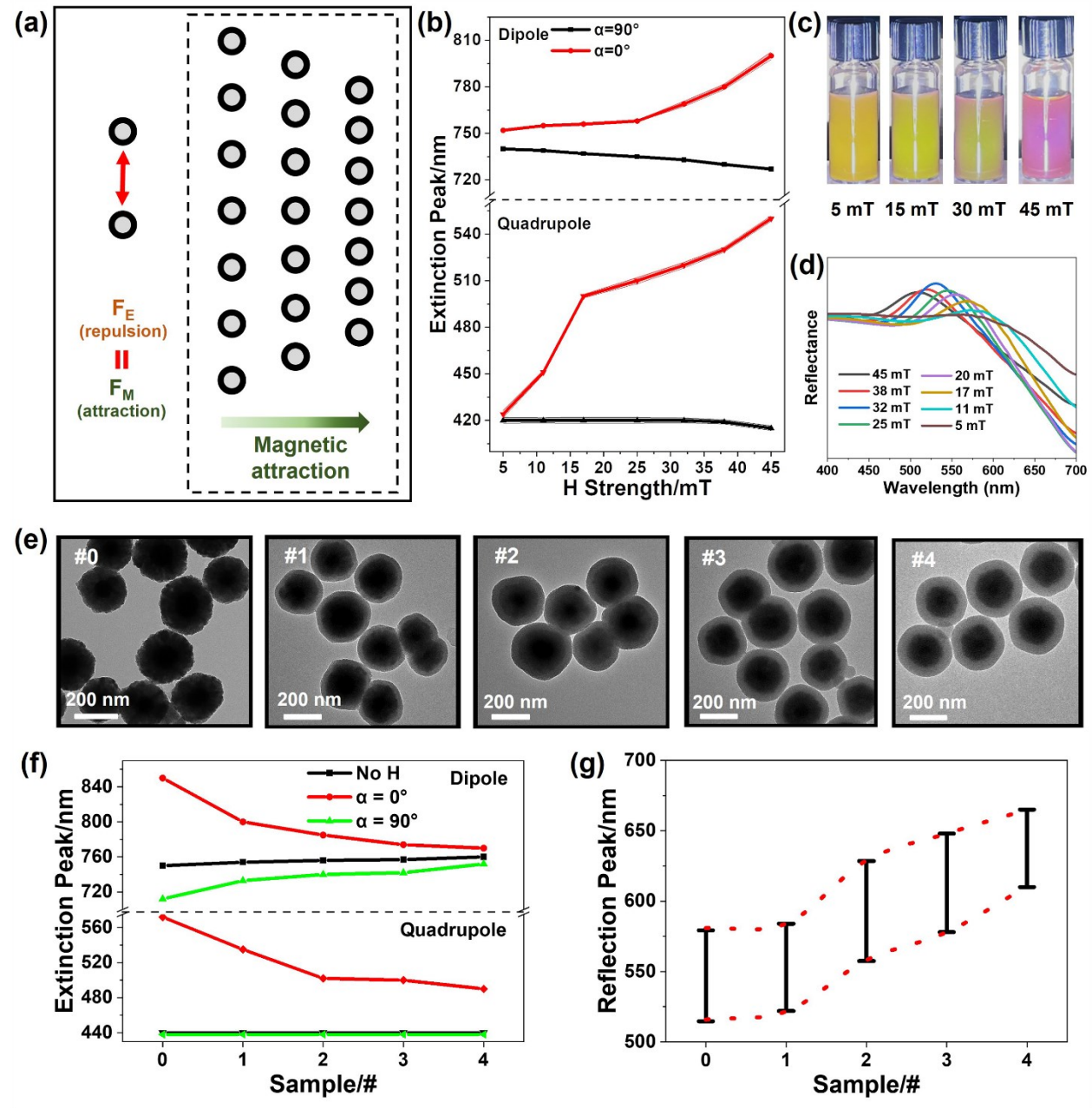


Figure 3. (a) Schematic illustration of the interaction between neighboring nanoparticles within a chain and the tunability of separation distance by controlling the magnetic field strength. (b) Extinction peak shifts of Ag@Fe₃O₄ nanoparticles under increasing magnetic field strength. (c, d) Color changes (c) and reflection peak shifts (d) under increasing magnetic field strength. (e) TEM images of the Ag@Fe₃O₄ nanoparticles before and after coating with silica shells of different thicknesses. (f) Extinction peak shifts of the 5 samples in (e) before and after exposure to a

magnetic field (45 mT) at $\alpha = 0$ and 90°. (g) Reflection peak tunability of the above 5 samples when the magnetic field changes from 5 to 45 mT at $\alpha = 0$ °.

Both plasmonic resonance and optical diffraction properties of the assembled structures can be dynamically tuned by controlling the interparticle separation by varying the magnetic field strength. As shown in Figure 3a, the interparticle distance is determined by the balance between electrostatic repulsion and magnetic attraction. As the magnetic field strength increases, the separation distance decreases. Both dipole and quadrupole plasmonic peaks were redshifted when α =0°, while they were slightly blueshifted when α =90° under a magnetic field of increasing strengths from 5 to 45 mT due to the stronger plasmonic coupling for shorter separation distance (Figure 3b). Figures 3c and d show the photos and reflection spectra of an aqueous solution of Ag@Fe₃O₄ nanoparticles in response to a magnetic field of varying strengths at α =0°. The color of the solution changed from yellow to green to purple, and the reflection peak blueshifted from 580 to 509 nm as the magnetic field strength increased from 5 to 45 mT. The interparticle distance was decreased from 300 to 263 nm, as estimated by Bragg's Law. As shown in Figure S10a, the increasing magnetic field strength induced the color changes from pink to purple and slight blueshift of the extinction and reflection peaks at α =90° (Figure S10b,c).

The interparticle separation is a critical factor that determines the diffraction wavelength of the periodic structures according to Bragg's law and also affects the plasmonic coupling between the neighboring nanoparticles. We have explored tuning the interparticle separation by coating the nanoparticles with a layer of silica of controlled thicknesses. As shown in the TEM images in Figure 3e and the dynamic light scattering (DLS) measurements (Figure S11d), Ag@Fe₃O₄ nanoparticles without (#0) and with silica shells of increasing thicknesses of 15 nm (#1), 25 nm (#2), 40 nm (#3), and 50 nm (#4) were synthesized. Under the same magnetic field strength (45

mT), with the increasing silica thickness, the separation distance increased, decreasing the plasmonic coupling and blueshifting both dipole and quadrupole peaks at α =0°. Only a slight redshift of the peaks was observed when α =90° (Figure 3f and S11). Figure 3g shows the tunable ranges of the reflection peak and the redshift of the ranges as the silica thicknesses increased under a magnetic field with varying strength from 5 to 45 mT at α =0°, consistent with the visual observations (Figure S12). For example, sample #1 showed tunable colors from yellow to green, while sample #4 showed red to yellow as the magnetic field strength increased from 5 to 45 mT.

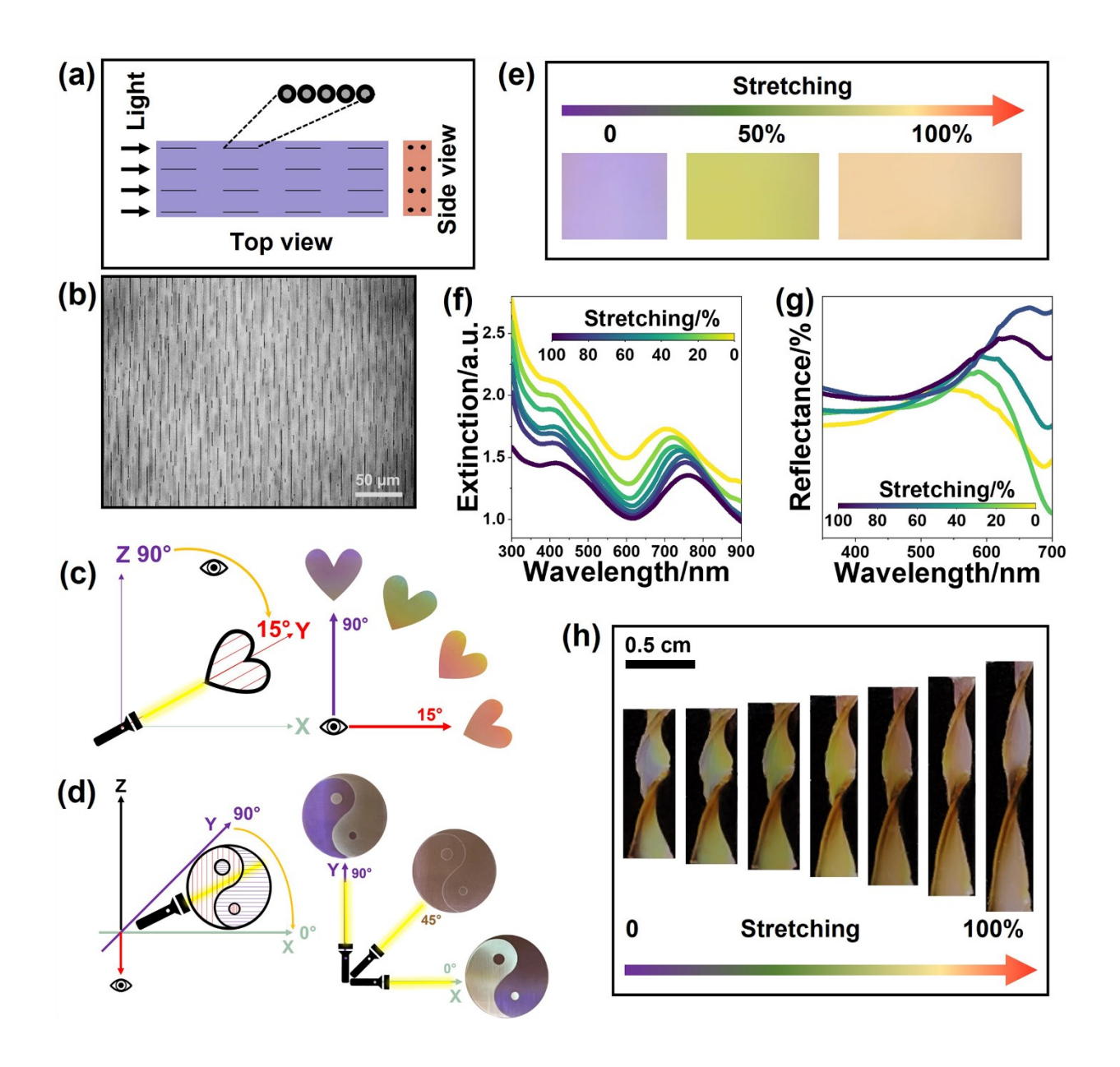


Figure 4. (a) Schematic illustration of the Ag@Fe₃O₄ nanoparticle chains fixed in the PAM hydrogel film. (b) Optical microscopic image of the Ag@Fe₃O₄ nanoparticle chains in the PAM hydrogel film. (c) Scheme and photo of color changes of a "heart" pattern when viewing angle varied from 90 to 15°. (d) Scheme and photo of a "Yin&Yang" pattern with the nanochain directions of the two regions perpendicular to each other, showing color switching when light direction changes from 0 to 90° in the XY plane. (e-g) Photos (e), extinction spectra (f), and reflection spectra (g) of the film upon stretching for 0 to 100%. (h) Photos of the twisted helical film under stretching for 0 to 100%.

The Ag@Fe₃O₄ nanochains can be fixed inside a polymer matrix to produce a photonic film with angular-dependent optical properties. The photonic film was fabricated through the magnetic assembly of Ag@Fe₃O₄ nanoparticles within an aqueous solution of acrylamide monomers, followed by a UV curing process. Figures 4a and b show that the nanoparticles assembled into 1D chains within a polyacrylamide (PAM) hydrogel, producing diffractive colors when the light was illuminated along the nanochain direction. The hydrogel film exhibited the same angulardependent optical properties as the nanochains solution (Figure S13). Figure 4c illustrates the nanochains' orientation (Y-axis), light propagation direction (Y-axis, parallel to nanochains), and the varying viewing angle from the Z- to the Y-axis. When the viewing angle decreased from 90 to 15° in the YZ plane, the color of the "heart" pattern changed from purple to green, yellow, and red. As an advantageous feature of the magnetic assembly strategy, the orientation of nanochains can be precisely controlled to produce complex patterns. Figure 4d schematically shows a "Yin&Yang" pattern with nanochains assembled along the Y-axis on the left and X-axis on the right halves, with the chains in reverse orientations for the small circles. The pattern was viewed along the Z-axis, and the incident direction was tuned within the XY plane. When the incident light was along the Y-axis (90°), the nanochains parallel to the light direction showed purple color, while the nanochains perpendicular to the light direction showed light blue. When the incident light propagated along the X-axis (0°), the colors on the left and right sides of the pattern were switched compared with the case when light propagated along Y-axis. Interestingly, the color difference disappeared when light propagated along 45° in the XY plane because both nanochains had the same angle (45°) relative to the light direction, indicating the potential application for information encryption (Video 3).

The elasticity of the polymer film also offers the possibility of tuning the photonic properties dynamically by mechanical stretching. Figure 4e shows the color changes of the film from purple to green to yellow upon stretching along the nanochain direction from 0 to 100%. The stretching induces the redshift of extinction and reflection peaks (Figures 4f and g), attributed to the increased lattice constant under stress. A more complex photonic film was fabricated by combining angular dependence and mechanical tunability into a single twisted film, showing different colors from different regions due to the angular-dependent property (Figure 4h). The color was also redshifted upon stretching.

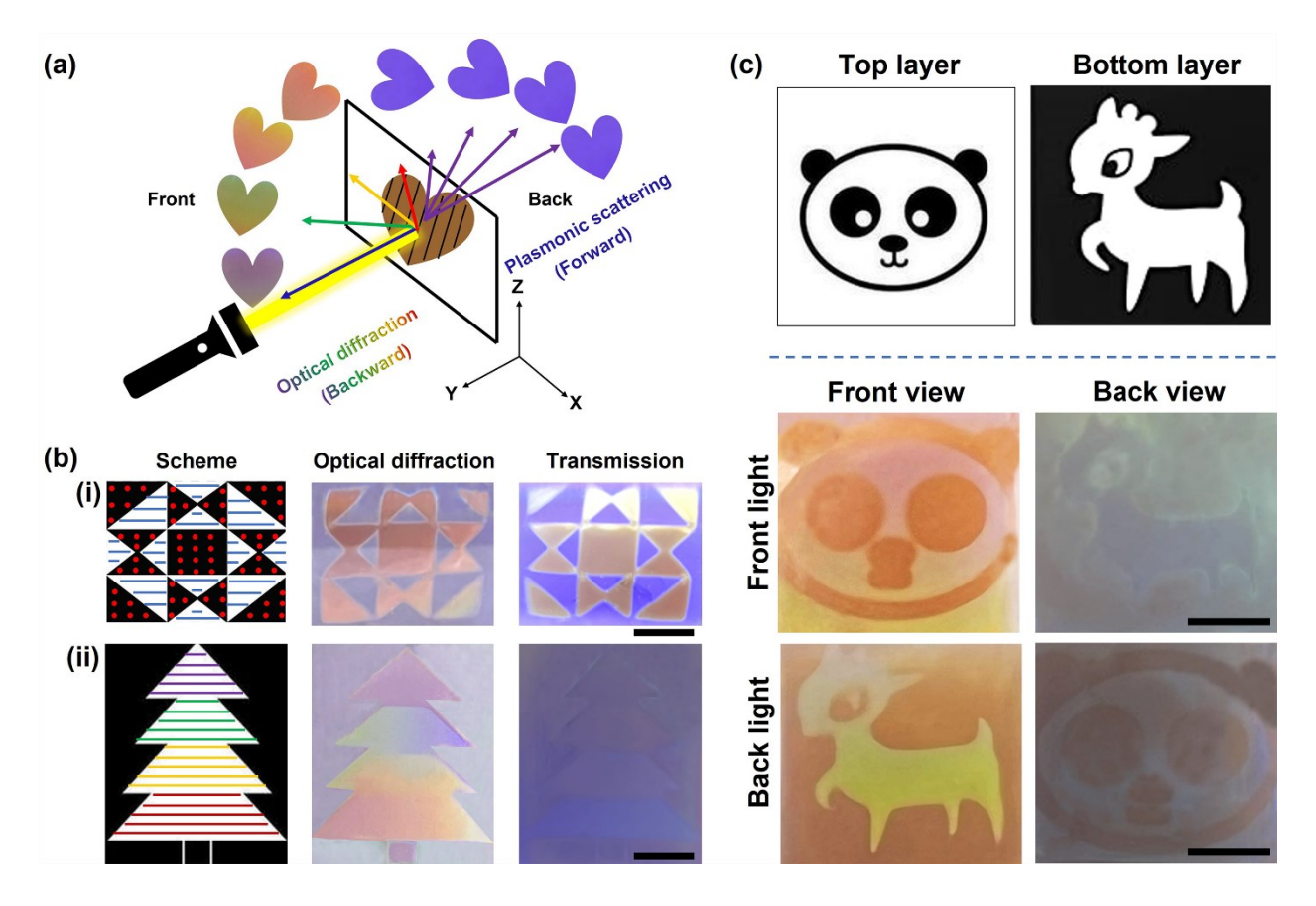


Figure 5. (a) Scheme and photos showing the angular-dependent reflective colors of a "heart" pattern due to the backward optical diffraction (front) and the angular-independent transmissive color due to the forward plasmonic scattering (back). (b) Thin films containing nanochains of designed orientations showing different patterns in reflectance and transmission modes: (i) a pattern with black and white regions containing nanochains with normal and parallel alignments to the film surface, respectively (scheme, left panel). Viewing from the front (photo, middle panel) sees diffractive color from black regions and plasmonic scattering color from the white regions. Observing from the backside (photo, right panel) sees light blue in the black regions and purple in the white regions. (ii) a tree pattern with regions containing nanochains with decreasing periodicities from bottom to top, showing blue shifts of diffractive colors when observed from the front side and purple plasmonic scattering color in all regions when viewed from the backside. (c) Scheme and photos of a double-layer film with a top "panda head" pattern and a bottom "deer"

pattern. Light irradiation from top to bottom reveals the "panda head" pattern for front observation due to optical diffraction and the "deer" pattern for back observation due to plasmonic scattering. The situation is reversed when light is irradiated from the bottom to the top. All the scale bars are 0.5 cm.

The photonic film can display dual colors when viewed from different sides: diffractive color from the front and plasmonic scattering color from the back. As shown in Figure 5a, the nanochains aligned along the Z-axis in a "heart" pattern, and light propagated along the Y-axis. When viewed from the front of the film, diffractive color dominated and showed angular-dependent colors from purple to red as the viewing direction varied from Y-axis to Z-axis. Only blue appeared under different viewing angles within the YZ plane when observed from the back of the film (Video 4). The color observed from the backside of the film was mainly from the plasmonic scattering and transmitted light, showing no angular dependence. By utilizing this unique optical property, many complicated patterns with intriguing appearances can be fabricated. Figure 5b(i) shows a pattern with black regions containing nanochains aligned perpendicularly to the plane while white regions containing nanochains parallel to the plane. Under light illumination, red was reflected from the black regions due to the optical diffraction, while purple appeared in white regions due to the plasmonic scattering when the film was viewed from the front. When observed from the backside, the black regions showed light brown, and the white regions appeared blue due to the angularindependent plasmonic scattering. Figure 5b(ii) shows a "tree" pattern with four different regions containing nanochains with the same orientation but decreasing periodicity from bottom to top, fabricated by applying increasing magnetic field strength while fixing the nanoparticles in the polymer matrix. When light illuminated along the nanochain direction, diffractive colors of red, yellow, green, and purple from the bottom to top regions were observed from the front. In contrast,

the photonic film was purple only due to plasmonic scattering with negligible difference between different regions because all the nanochains were aligned along the same orientation.

More functional photonic films can be achieved by stacking two patterned films together. As shown in Figure 5c, a double-layer film was fabricated by combining two films with a "panda head" pattern on the top and a "deer" pattern at the bottom. Under top illumination, only the "panda head" appeared with a diffractive color when viewed from the front, while only the "deer" pattern could be observed with purple color due to plasmonic scattering when observed from the backside. The situation was reversed when the light was illuminated from the back, showing only the diffractive color of the "deer" pattern and the plasmonic scattering color of the "panda head" as observed from the back and front sides, respectively. Combining backward optical diffraction and forward plasmonic scattering in a single system allows the exploration of the potential for designing multi-functional color displays and optical devices.

In summary, we have developed unique angular-dependent and dynamically tunable 1D plasmonic photonic crystals by assembling magneto-plasmonic nanoparticles under an external magnetic field. The combination of plasmonic resonance, photonic bandgap, and magnetic assembly enables precise modulation of the optical properties in real time by controlling the interplay between the plasmonic and diffraction modes. The magnetic assembly process allows convenient and instant organization of Ag@Fe₃O₄ nanoparticles into chains, the precise manipulation of their interparticle separation, and fixation in the elastic polymer matrix with controlled orientation. Photonic films of complex patterns could be fabricated with angular-dependent and mechanically tunable optical properties, promising for broad applications in color displays, optical devices, and information encryption. It is envisioned that more interesting optical properties can be achieved by varying the composition and morphology of the plasmonic cores in the hybrid nanostructures.³⁶⁻³⁷

ASSOCIATED CONTENT

Supporting Information is available free of charge.

Materials and synthesis of Ag@Fe₃O₄ nanoparticles, the surface modification with PAA and silica

coating, method of fixing nanochains within a polymer matrix, characterization methods, FTTD

simulation method, figures showing size distribution of the nanoparticles, extinction spectra and

electric field of single nanoparticle and nanochains, optical image of the magnetically assembled

1D nanochains, TEM, photo images and extinction spectra of Ag and Fe₃O₄ hollow nanoparticle

solutions, calculation according to Bragg's Law, photo images and reflection spectra of silica

coated nanoparticles, and photo images, extinction and reflection spectra of photonic films.

AUTHOR INFORMATION

Corresponding Author

Yadong Yin- Department of Chemistry, University of California, Riverside, CA 92521, USA

E-mail: yadong.yin@ucr.edu

Author Contributions

Y.Y. and C.W. designed this project. C.W. performed the experiments. Y.L. and T.L. synthesized

the nanoparticles. Q.F., W.W., and H.Y. performed FDTD simulation. The manuscript was written

by C.W. and revised by Y.Y. All authors have approved the final version of the manuscript.

Funding Sources

U.S. National Science Foundation (CHE- 2203972)

ACKNOWLEDGMENT

17

We are grateful for the financial support from the U.S. National Science Foundation (CHE-2203972).

REFERENCES

- 1. Zi, J.; Yu, X.; Li, Y.; Hu, X.; Xu, C.; Wang, X.; Liu, X.; Fu, R., Coloration strategies in peacock feathers. *Proceedings of the National Academy of Sciences* **2003**, *100* (22), 12576-12578.
- 2. Gralak, B.; Enoch, S., Structural colors in nature and butterfly-wing modeling. *Optics and photonics news* **2003**, *14* (2), 38-43.
- 3. Chung, K.; Yu, S.; Heo, C. J.; Shim, J. W.; Yang, S. M.; Han, M. G.; Lee, H. S.; Jin, Y.; Lee, S. Y.; Park, N., Flexible, angle-independent, structural color reflectors inspired by Morpho butterfly wings. *Advanced Materials* **2012**, *24* (18), 2375-2379.
- 4. Zhao, Y.; Xie, Z.; Gu, H.; Zhu, C.; Gu, Z., Bio-inspired variable structural color materials. *Chemical Society Reviews* **2012**, *41* (8), 3297-3317.
- 5. Shang, L.; Zhang, W.; Xu, K.; Zhao, Y., Bio-inspired intelligent structural color materials. *Materials Horizons* **2019**, *6* (5), 945-958.
- 6. Kim, H.; Choi, J.; Kim, K. K.; Won, P.; Hong, S.; Ko, S. H., Biomimetic chameleon soft robot with artificial crypsis and disruptive coloration skin. *Nature communications* **2021**, *12* (1), 1-11.
- 7. Xuan, Z.; Li, J.; Liu, Q.; Yi, F.; Wang, S.; Lu, W., Artificial structural colors and applications. *The Innovation* **2021**, *2* (1), 100081.
- 8. Daqiqeh Rezaei, S.; Dong, Z.; You En Chan, J.; Trisno, J.; Ng, R. J. H.; Ruan, Q.; Qiu, C.-W.; Mortensen, N. A.; Yang, J. K., Nanophotonic structural colors. *ACS Photonics* **2020**, *8* (1), 18-33.
- 9. Chen, F.; Wang, S.-W.; Liu, X.; Ji, R.; Li, Z.; Chen, X.; Chen, Y.; Lu, W., Colorful solar selective absorber integrated with different colored units. *Optics express* **2016**, *24* (2), A92-A103.
- 10. Fan, W.; Zeng, J.; Gan, Q.; Ji, D.; Song, H.; Liu, W.; Shi, L.; Wu, L., Iridescence-controlled and flexibly tunable retroreflective structural color film for smart displays. *Science Advances* **2019**, *5* (8), eaaw8755.
- 11. Kim, S.; Mitropoulos, A. N.; Spitzberg, J. D.; Tao, H.; Kaplan, D. L.; Omenetto, F. G., Silk inverse opals. *Nature Photonics* **2012**, *6* (12), 818-823.
- 12. Li, W.; Wang, Y.; Li, M.; Garbarini, L. P.; Omenetto, F. G., Inkjet printing of patterned, multispectral, and biocompatible photonic crystals. *Advanced Materials* **2019**, *31* (36), 1901036.
- 13. Kristensen, A.; Yang, J. K.; Bozhevolnyi, S. I.; Link, S.; Nordlander, P.; Halas, N. J.; Mortensen, N. A., Plasmonic colour generation. *Nature Reviews Materials* **2016**, *2* (1), 1-14.
- 14. Kinoshita, S.; Yoshioka, S.; Miyazaki, J., Physics of structural colors. *Reports on Progress in Physics* **2008,** *71* (7), 076401.
- 15. Goodling, A. E.; Nagelberg, S.; Kaehr, B.; Meredith, C. H.; Cheon, S. I.; Saunders, A. P.; Kolle, M.; Zarzar, L. D., Colouration by total internal reflection and interference at microscale concave interfaces. *Nature* **2019**, *566* (7745), 523-527.
- 16. Yang, W.; Xiao, S.; Song, Q.; Liu, Y.; Wu, Y.; Wang, S.; Yu, J.; Han, J.; Tsai, D.-P., All-dielectric metasurface for high-performance structural color. *Nature communications* **2020**, *11* (1), 1-8.
- 17. Ge, J.; Yin, Y., Responsive photonic crystals. *Angewandte Chemie International Edition* **2011,** *50* (7), 1492-1522.
- 18. Wang, H.; Brandl, D. W.; Nordlander, P.; Halas, N. J., Plasmonic nanostructures: artificial molecules. *Accounts of chemical research* **2007**, *40* (1), 53-62.
- 19. Li, Z.; Wang, W.; Yin, Y., Colloidal assembly and active tuning of coupled plasmonic nanospheres. *Trends in Chemistry* **2020**, *2* (7), 593-608.

- 20. Li, Z.; Wang, M.; Zhang, X.; Wang, D.; Xu, W.; Yin, Y., Magnetic assembly of nanocubes for orientation-dependent photonic responses. *Nano Letters* **2019**, *19* (9), 6673-6680.
- 21. Li, Z.; Fan, Q.; Yin, Y., Colloidal self-assembly approaches to smart nanostructured materials. *Chemical Reviews* **2021**, *122* (5), 4976-5067.
- 22. Romanov, S. G.; Korovin, A. V.; Regensburger, A.; Peschel, U., Hybrid colloidal plasmonic-photonic crystals. *Advanced Materials* **2011**, *23* (22-23), 2515-2533.
- 23. Yu, X.; Shi, L.; Han, D.; Zi, J.; Braun, P. V., High quality factor metallodielectric hybrid plasmonic—photonic crystals. *Advanced Functional Materials* **2010**, *20* (12), 1910-1916.
- 24. Kim, J. B.; Kim, J. W.; Kim, M.; Kim, S. H., Dual-Colored Janus Microspheres with Photonic and Plasmonic Faces. *Small* **2022**, 2201437.
- 25. Wang, Y.; Kim, B. J.; Guidetti, G.; Omenetto, F. G., Generation of Complex Tunable Multispectral Signatures with Reconfigurable Protein-Based, Plasmonic-Photonic Crystal Hybrid Nanostructures. *Small* **2022**, 2201036.
- 26. Li, Z.; Yang, F.; Yin, Y., Smart materials by nanoscale magnetic assembly. *Advanced Functional Materials* **2020**, *30* (2), 1903467.
- 27. He, L.; Wang, M.; Ge, J.; Yin, Y., Magnetic assembly route to colloidal responsive photonic nanostructures. *Accounts of chemical research* **2012**, *45* (9), 1431-1440.
- 28. Ge, J.; He, L.; Hu, Y.; Yin, Y., Magnetically induced colloidal assembly into field-responsive photonic structures. *Nanoscale* **2011**, *3* (1), 177-183.
- 29. Ge, J.; Yin, Y., Magnetically responsive colloidal photonic crystals. *Journal of Materials Chemistry* **2008**, *18* (42), 5041-5045.
- 30. Luo, W.; Ma, H.; Mou, F.; Zhu, M.; Yan, J.; Guan, J., Steric-Repulsion-Based Magnetically Responsive Photonic Crystals. *Advanced Materials* **2014**, *26* (7), 1058-1064.
- 31. Wang, M.; Gao, C.; He, L.; Lu, Q.; Zhang, J.; Tang, C.; Zorba, S.; Yin, Y., Magnetic tuning of plasmonic excitation of gold nanorods. *Journal of the American Chemical Society* **2013**, *135* (41), 15302-15305.
- 32. Li, Z.; Jin, J.; Yang, F.; Song, N.; Yin, Y., Coupling magnetic and plasmonic anisotropy in hybrid nanorods for mechanochromic responses. *Nature communications* **2020**, *11* (1), 1-11.
- 33. Li, Z.; Fan, Q.; Wu, C.; Li, Y.; Cheng, C.; Yin, Y., Magnetically tunable plasmon coupling of Au nanoshells enabled by space-free confined growth. *Nano Letters* **2020**, *20* (11), 8242-8249.
- 34. Zhang, Y.; Ding, H.; Liu, Y.; Pan, S.; Luo, Y.; Li, G., Facile one-step synthesis of plasmonic/magnetic core/shell nanostructures and their multifunctionality. *Journal of Materials Chemistry* **2012**, *22* (21), 10779-10786.
- 35. Song, Y.; Tran, V.; Lee, J., Tuning plasmon resonance in magnetoplasmonic nanochains by controlling polarization and interparticle distance for simple preparation of optical filters. *ACS applied materials & interfaces* **2017**, *9* (29), 24433-24439.
- 36. Pang, X.; Zhao, L.; Han, W.; Xin, X.; Lin, Z., A general and robust strategy for the synthesis of nearly monodisperse colloidal nanocrystals. *Nature nanotechnology* **2013**, *8* (6), 426-431.
- 37. Pang, X.; He, Y.; Jung, J.; Lin, Z., 1D nanocrystals with precisely controlled dimensions, compositions, and architectures. *Science* **2016**, *353* (6305), 1268-1272.

TOC Graphic:

